Solar Energy Materials & Solar Cells 166 (2017) 212–221

Contents lists available at ScienceDirect

Solar Energy Materials & Solar Cells

journal homepage: www.elsevier.com/locate/solmat

Solvent-engineering assisted synthesis and characterization of $BiVO_4$ photoanode for boosting the efficiency of photoelectrochemical water splitting

Truong-Giang Vo[a,b], Jian-Ming Chiu[b], Chia-Ying Chiang[a,*], Yian Tai[b,*]

[a] Sustainable Engineering Lab, Department of Chemical Engineering, National Taiwan University of Science and Technology, Taiwan ROC
[b] Nanohybrid Materials and Devices Lab, Department of Chemical Engineering, National Taiwan University of Science and Technology, Taiwan ROC

ARTICLE INFO

Keywords:
Bismuth vanadate
Ethylene glycol
Photoelectrochemical cell
Water splitting

ABSTRACT

A simple direct, scalable and reproducible approach for preparing photoelectrochemically active $BiVO_4$ films on fluorine-doped tin oxide (FTO) substrates by hydrothermal method using a mixing solvent of ethylene glycol/water was presented for the first time. As-prepared $BiVO_4$ thin films were found to have pure monoclinic scheelite structure with a compact, irregular microstructured morphology and strong absorption in the visible-light region with estimated bandgap of 2.4 eV. When applied as an electrode material for water splitting in borate electrolyte solution, a significantly enhanced stability, coupled with a 15-fold increase in photocurrent density (*ca.* 1.04 mA cm^{-2}) are observed compared to those of conventional hydrothermal synthesized films. The $BiVO_4$ prepared with mixed solvent gave a substantial enhancement of the incident photon to current efficiency (IPCE) and absorbed photon to current efficiency (APCE) during light driven oxygen evolution reaction.

1. Introduction

Over the past few decades, many scientists and engineers have dedicated substantial efforts exploiting and developing efficient photocatalysts to deal with energy and environmental problems which have threatened the modern society. Till now, as benchmark materials for photoconversion processes, titanium dioxide (TiO_2) and zinc oxide (ZnO) have been intensively studied for this purpose owing to their high efficiency, nontoxicity, high stability, environmentally friendly and inexpensive materials [1–3]. Nevertheless, their advantageous properties are offset by the fact that they are incapable of absorbing visible light and have high recombination rate of photo-excited species [4,5]. Therefore, many other material systems which absorb visible light such as CdS [6], PdS [7], Se-based compounds ($NiSe_2$, $CoSe_2$, $PdSe_2$) [8] have been recently developed. However, practically they are barely applicable because of the elemental toxicity and accompanied environmental issues during preparation and disposal processes [9,10]. Among various visible-light responsive materials, the binary metal oxide, bismuth vanadate ($BiVO_4$), has been recognized as one of the most promising materials because of its earth abundant, relatively intoxicity, and high stability against chemical and photoelectrochemical (PEC) corrosion [11,12]. Among three $BiVO_4$ polymorphs (monoclinic, tetragonal and tetragonal-zircon structures), it is well-known that only monoclinic $BiVO_4$ with relatively low band gap (2.2–2.5 eV) [5,12] shows excellent photocatalytic performance in the decomposition of organic pollutants and photocatalytic evolution of oxygen under visible light irradiation [3,13]. Additionally, it provides well-positioned band edges (conduction band and valence band at ~0 and 2.4 V *vs.* RHE, respectively) and requires relatively low onset potential for water oxidization [14]. Hence, monoclinic $BiVO_4$ has been intensively and widely studied for use in both photocatalytic and photoelectrocatalytic applications in recent years.

This interest in $BiVO_4$ has led to a considerable amount of works on the synthesis of $BiVO_4$ bulks. Although it is beneficial for in-depth analysis of crystal properties, bulk powders are unsuitable for the practical applications. This drawback has led to a considerable amount of works on the preparation of $BiVO_4$ films over a conductive substrate. There are many approaches for the fabrication of $BiVO_4$ on a substrate, including metal organic decomposition [15–19], chemical vapor deposition [20], chemical bath deposition [21], dip coating [22], spray pyrolysis [23], and electrodeposition [24,25]. It cannot be denied that each of these above methods has certain advantages, but they also face some obstacles such as poor substrate adhesion, high reaction temperature (500 °C) or complicate post-treatment [26]. For instance,

* Corresponding authors.
E-mail addresses: cychiang@mail.ntust.edu.tw (C.-Y. Chiang), ytai@mail.ntust.edu.tw (Y. Tai).

http://dx.doi.org/10.1016/j.solmat.2017.03.012
Received 25 October 2016; Received in revised form 7 March 2017; Accepted 14 March 2017
Available online 30 March 2017

Kang et al. have described the poor adhesion and coverage of $BiVO_4$ deposited on conducting glass, fluorine-doped tin oxide (FTO), by electrodeposition method [25]. Luo et al. reported a procedure to fabricate $BiVO_4$ microelectrode by chemical bath deposition that requires post-annealing at 580 °C for 24 h [21]. Alarcón-Lladó and coworkers presented the synthesis of $BiVO_4$ by chemical vapor deposition using even higher temperature of 900 °C [20]. Such high temperature process limits the option of substrates that can be utilized. To solve those difficulties, herein, we report a simple, convenient, relatively low temperature, and reproducible hydrothermal treatment process for fabricating $BiVO_4$ thin film on FTO substrate. The hydrothermal method has advantages over other wet chemistry methods, including the potential for generating highly crystalline and narrow size distribution products, and high morphology control ability by tuning process parameters or precursor compositions [27]. Simultaneously, ethylene glycol (EG) is widely accepted as a green solvent with high viscosity and chelate ability which can control crystal growth. In the present study, we employed a mixture of water and EG as solvent for the hydrothermal synthesis of $BiVO_4$. This approach results in a dense, homogeneous and high crystalline hydrophilic $BiVO_4$ film with robust substrate adhesion, leading to remarkable PEC performances.

2. Experimental

2.1. Materials

FTO-coated glass (15 Ω/sq, 14 mm×18 mm) was employed as the substrate for thin film electrode fabrication. $Bi(NO_3)_3{\cdot}5H_2O$ (Acros, 99.9%), NH_4VO_3 (Alfa Aesar, 98%), $VO(acac)_2$ (Strem, 98%), acetic acid (Sigma, 99.7%), 2,4-pentanedione (Sigma, 99.5%), HNO_3 (Sigma, 65%), NaOH (Sigma, 97%), ethylene glycol (Acros, 99.9%), $Na_2B_4O_7$ (Showa, 99%) were used directly without any further purification.

2.2. Fabricating $BiVO_4$ film

FTO-coated glass was cleaned by sonication in de-ionized (DI) water, acetone and isopropanol alcohol (20 min each), and following by nitrogen (N_2) gas flux drying. To orientate and to boost high-density growth, a seed layer was deposited on FTO-coated glass by previous spin-coating procedures [16] with slight modification. The spin-coating precursor was made as follows. Equimolar amounts of bismuth nitrate ($Bi(NO_3)_5{\cdot}5H_2O$, 0.25 mmol) and vanadyl acetylacetonate ($VO(AcAc)_2$, 0.25 mmol) were added to a 5 mL solution of 1:8.25 acetic acid and 2,4-pentanedione, following by sonication for 15 min to obtain the stable dark green solution. Prior to coating, the resulting solution was filtered with a 0.22 μm nylon filter (Thermo Scientific), then a small amount of precursor solution being spread over an area of 0.64 cm^2 in the FTO substrate (previously masked with the aids of Scotch tapes to leave some non-coated FTO available for the electrical contacts). Spin coating parameters were set at 2500 rpm for 20 s. After drying in air, coated glass was annealed in a muffle furnace at 500 °C for 10 min with the ramping rate of 2 °C min^{-1}.

The synthetic route of $BiVO_4$ films is illustrated in Fig. 1a. In a typical synthesis procedure, for control purpose, 1.0 mmol $Bi(NO_3)_3{\cdot}5H_2O$ was dissolved in 20 mL of HNO_3 1 M and 10 mL of ethylene glycol (EG) to form solution A. Meanwhile, 1.0 mmol NH_4VO_3 was dissolved in 20 mL of NaOH 0.5 M and 10 mL of EG to form solution B. After stirring for 30 min at room temperature, solution B was added slowly to solution A with continuous stirring for an additional 30 min. A piece of FTO glass slide (14 mm x 18 mm) was then immersed in this yellow suspension with its conductive side down. Afterward, the 60 mL of the mixture was transferred to a 100 mL Teflon-lined stainless autoclave and then put in an oven at 180 °C under autogenous pressure for 12 h. After that, the autoclave was cooled naturally to ambient temperature, the sample was taken out and washed with acetone and blown dry using an N_2 stream. For convenience, $BiVO_4$ film prepared from the mixed solvent system was termed as MIX-BVO. Also, to confirm the effect of EG, the comparative experiments using pure water without EG (denoted as H_2O-BVO) and pure EG without water (EG-BVO) were also carried out. It should be mentioned that for a fair comparison in phototoelectrochemical performance, H_2O-BVO samples with relatively controlled thickness were grown by adjusting the hydrothermal deposition duration time while keeping other parameters constant.

2.3. Morphology and crystal structure characterization

The morphology of the samples prepared as described above was analyzed by field emission scanning electron microscope (JEOL JSM6700) equipped with an energy-dispersive X-ray spectroscopy (EDS) analysis, which was employed to obtain an insight of the bulk element composition of the sample. The crystal phase of as-synthesized samples was characterized by Bruker D2 Phaser XRD in the region of 2θ=10–70° using Cu Kα radiation (λ=0.15418 nm) with a step size a 0.02° and a scanning rate at 0.1° s^{-1}. The absorption spectra and the light-harvesting efficiency (LHE) of the electrode were measured and calculated using a doubled-beam ultraviolet-visible (UV–Vis) spectrophotometer (Jasco V670, Japan) using bare FTO as a reference. The Raman spectra and images were taken with a microscopic Raman system (MRI, Protrustech Co, Ltd., Taiwan). The 532-nm line of a laser with a laser power of 50 mW was used as the excitation wavelength. A motorized xy stage was applied for Raman mapping, a technique that yields information on the spatial distribution of the different crystalline parts that are located on the surfaces of the film. The photoluminescence (PL) spectra of the samples were recorded on Fluorolog-Tau-3 spectrofluorometer (Jobin Yvon, USA) with an excitation wavelength of 325 nm. X-ray photoelectron spectroscopy (XPS) (VG ESCA Scientific Theta Probe & VG Scientific ESCALAB 250) was used for the surface element composition analysis.

2.4. PEC measurements

The PEC performance of synthesized $BiVO_4$ electrodes as photoanodes for water oxidation reaction was carried out in a three-electrode, single-compartment quartz cell connecting with an electrochemical analyzer potentiostat (Autolab PGSTAT302N, Switzerland). Notably, the PEC cell has two sides of quartz for preventing light absorbance. The $BiVO_4$ thin film with working area of 0.64 cm^2 (8 mm for both length and width) was used as the working electrode while a 2.5 cm×2.5 cm Pt mesh (100 mesh) and an Ag/AgCl (3 M KCl) electrode were employed as counter and reference electrodes, respectively. 0.1 M $Na_2B_4O_7$ aqueous solution (pH 9.3) was used as the electrolyte. In the cases of studying $BiVO_4$ surface reaction kinetics, 0.1 M sodium sulfite (Na_2SO_3) was added into the electrolyte as a hole scavenger. Linear scan voltammetry (LSV) was conducted in the dark and under irradiation by a solar simulator with a 300 W Xenon lamp (Model 66905, Newport) and an AM 1.5 G filter. The light intensity of the lamp was calibrated with a reference silicon solar cell and a readout meter for solar simulator irradiance (Model 91,150 V, Newport) to warrant that light intensity was fixed at 100 mW cm^{-2} in all experiments. Unless stated otherwise, the light was irradiated through the $BiVO_4$ semiconductor side (front-side). Photocurrents were measured while sweeping the potential from −0.6 to 0.7 V *vs.* Ag/AgCl (3 M KCl) in the positive direction with a scan rate of 10 mV s^{-1} and step potential of 0.0244 V. At least three samples were tested to obtain the significant statistical results for all experiments unless otherwise noted. Cyclic voltammetry (CV) scans were performed for five cycles with similar settings as described for LSVs. Mott-Schottky plot was obtained by using a potentiostat (Autolab, Netherlands) in the dark with the applied frequency of 1 kHz and amplitude of 10 mV. The electrochemical impedance spectroscopy (EIS) were conducted at 0.5 V *vs.* Ag/AgCl with an AC amplitude of 10 mV, frequency of 100 kHz–

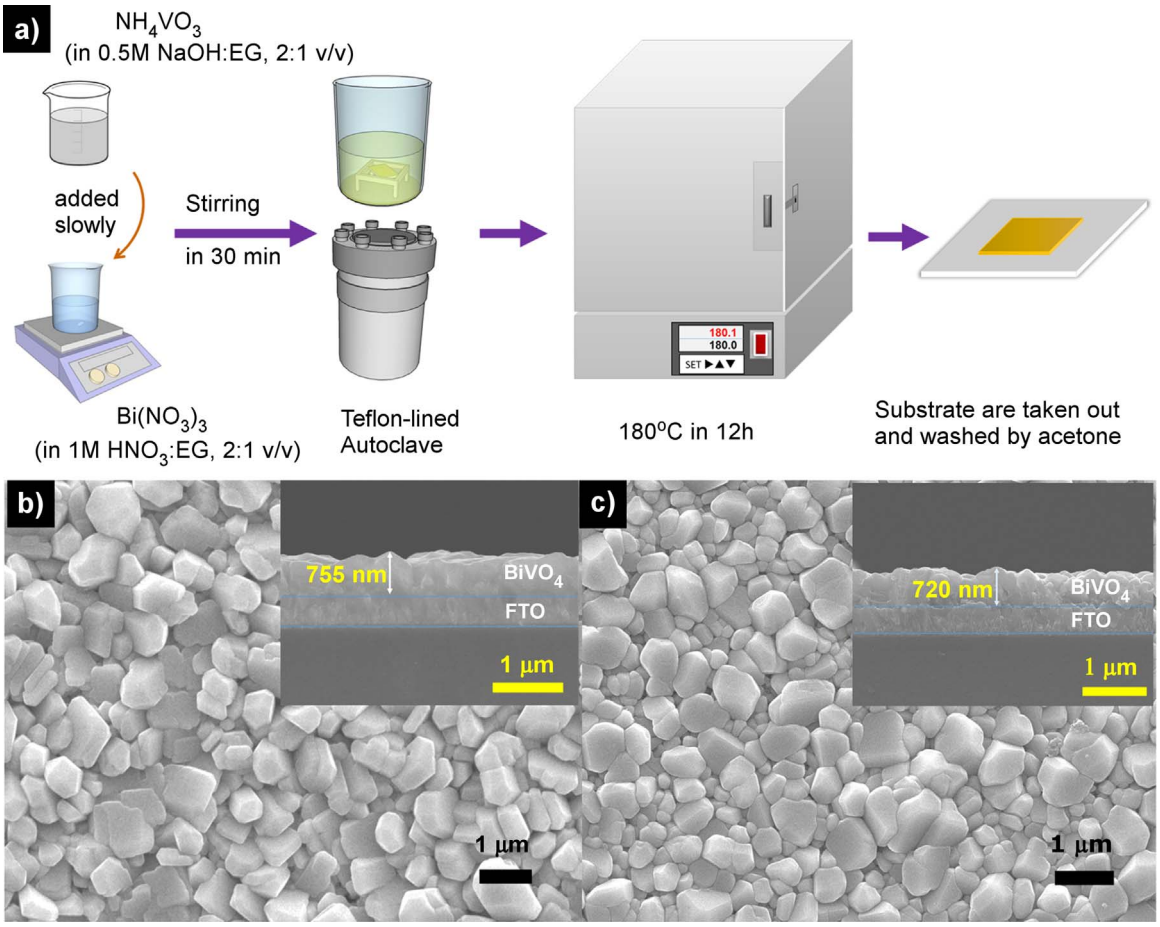

Fig. 1. (a) Schematic diagram illustrating the synthetic route of $BiVO_4$ films. (b, c) SEM images of H_2O-BVO and MIX-BVO films (b). The inset of (b, c) shows the corresponding side-view.

100 mHz, under the above reported simulated sunlight conditions. The electrolyte solution was purged with N_2 for 30 min to remove dissolved oxygen in advance. The measured spectra were fitted by using the Nova software package (Nova version 1.10). For measurement of the power output characteristics and photon to current efficiency, a two-electrode configuration consisting of the $BiVO_4$ photoelectrode and Pt as the counter electrode was used. The reference electrode of the electrochemical workstation was short-circuited with the counter-electrode of the PEC cell. The incident photon to current efficiency (IPCE) was obtained by a solar cell monochromatic incident photon-to-electron conversion efficiency measurement system (SCS10-X150-DSSC, Zolix) with an externally applied bias of 1 V *versus* a Pt counter electrode at the similar condition as described above for photoelectrochemical tests. Absorbed photon to current conversion efficiency (APCE) was obtained by dividing the IPCE by LHE at each wavelength.

The stability of $BiVO_4$ photoanode for oxygen evolution reaction was evaluated by chronoamperometry with a controlled potential at +0.6 V *vs.* Ag/AgCl for 1 h while the solution was stirred at 300 rpm. All potentials in this study were converted into reversible hydrogen electrode (RHE) scale for easy comparison with H_2 and O_2 redox potentials and other reports that use electrolytes with different pH conditions. The conversion between potentials *vs.* Ag/AgCl and *vs.* RHE was performed using the Eq. (1).

$$E_{RHE}=E_{Ag/AgCl}+0{\cdot}197\ V+0.059\ pH \quad (1)$$

3. Results and discussion

3.1. Characterization of the $BiVO_4$ films

The morphology of the $BiVO_4$ seed layer and the resulting $BiVO_4$ films thereafter on FTO were investigated by field emission scanning electron microscopy (FESEM) as presented in Fig. 1 and Fig. S2, respectively. As expected, for seed layer, a porous network of nanocrystals with the size in the range of 100–200 nm can be observed (Fig. S2). The cross-sectional SEM profiles of $BiVO_4$ seed layer (Fig. S2) showed no clear boundary between FTO and seed layer, suggesting that an extremely thin $BiVO_4$ seed layer was grown on the FTO substrates. Alpha-step measurement (Fig. S3) was employed for further confirming the average thickness of seed layer which was found to be around 55 nm. The top-view of Fig. 1b and c highlight the different morphologies of prepared $BiVO_4$ samples. When the binary solvent of EG/water was used, as-prepared MIX-BVO film consists of densely packed crystals with size in the range of 200 nm to 1 µm. On the other hand, the crystals of the H_2O-BVO become larger in size and arranged more loosely (Fig. 1b). Notably, when EG used as the unique solvent under hydrothermal treatment, as-obtained black large near-spherical crystals with tiny irregular particles were not grown uniformly on the substrate (Fig. S4a). The change in color of the film from yellow to dark brown probably due to the formation of other metal oxides instead of $BiVO_4$. The thicknesses of MIX-BVO and H_2O-BVO presented in the insets of Fig. 1b and c were approximately 720 ± 40 nm and 755 ± 35 nm, respectively. It should be mentioned that in the same hydrothermal treatment time a much thicker film (approximately 1.3 µm) with a higher degree of roughness of H_2O-BVO was observed due to its

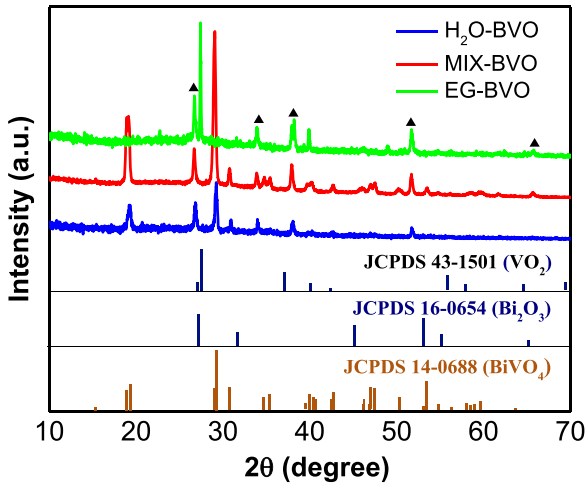

Fig. 2. XRD patterns of different $BiVO_4$ films. Peaks marked with black filled triangle correspond to SnO_2 from FTO substrate.

faster kinetic growth mechanism (Fig. S4b).

Notably, both H_2O-BVO and MIX-BVO were mechanically robust. The films neither come off even when subjected to wiping with tissue paper nor rub or scratch by a finger. More systematically, as shown in Fig. S5, tape-and-peel test (ASTM D3308) was performed. It is clearly observed that both $BiVO_4$ films firmly adhere to the substrate and have tightly bound crack-free grains, demonstrating the high reliability of hydrothermal synthesized $BiVO_4$ films towards usage under mechanically severe conditions. Furthermore, the complete coverage of substrates provides a favorable contribution to PEC activity since it can diminish the internal short circuit [28].

X-ray Diffraction (XRD) was performed to examine the existence of various $BiVO_4$ crystal phases. Fig. 2 represented XRD patterns of $BiVO_4$ films deposited on FTO glass. As compared with JCPDS 14-0688 standard profile, it is confirmed that as-synthesized MIX- and H_2O-BVO films are monoclinic $BiVO_4$, viz, the peaks position of 2θ are at 18.8°, 28.8°, 30.5°, 35.2°, 39.7°, 46.7° and 53.1°, which are characteristic peaks of m-$BiVO_4$, distinguishing from the tetragonal structure. Neither diffraction peaks from any other phased of $BiVO_4$ nor other metal oxides were observed for MIX- and H_2O-BVO, which points out the high selectivity of the chosen synthesis method towards the visible-light active monoclinic phase of $BiVO_4$. The lower intensity of diffraction peaks which implies the lower crystallinity of H_2O-BVO is due to a shorter hydrothermal treatment time. XRD data of all films also shows diffraction peaks assigned to SnO_2 from the FTO substrate (JCPDS 041-1445) underneath which marked by filled triangles because the BVO films were relatively thin. On the other hand, the major detectable diffraction peaks of the EG-BVO suggest that other oxides of bismuth and vanadium were generated, which consistent with the results of another report [29].

For a thorough analysis of the homogeneity and the quality of the crystallization process, the spatial distribution of the crystallized region was explored by performing 2D Raman mapping. A complete spectrum is acquired at each and every pixel of the image and then interrogated to generate false color images based on crystallinity (Fig. 3). The different in colors represents different intensity which implies the different in crystallization levels. As expected, MIX-BVO film exhibits the homogeneous distribution with high crystalline $BiVO_4$ as compared with H_2O-BVO sample (inset of Fig. 3). This feature is believed to play a critical role in enhancing the photocatalytic activity of $BiVO_4$ film. In order to obtain further insights into the crystalline and local structure of $BiVO_4$ layer. The Raman spectrum in the 200–1000 cm^{-1} region in the fully and partially crystallized parts was also presented in Fig. 3. The spectra show good agreement with those previous reports [30,31] for scheelite monoclinic $BiVO_4$ that have typical and distinctive vibrational bands at about 210, 335, 368, 718 and 824 cm^{-1}. The band centered at 210 cm^{-1} can be contributed to the lattice vibrations (rotation/translation) of $BiVO_4$. Set of medium intensity peaks centered at 368 and 335 cm^{-1} is due to the typical symmetric and asymmetric bending modes of the vanadate anion, respectively. The dominated peak at 824 cm^{-1} and an inconspicuous shoulder at 718 cm^{-1}, are the symmetric and asymmetric V–O stretching modes, respectively. Raman investigations point out that films synthesized with mixed solvent show better crystallinity than samples prepared with only water. Notably, it is reported that the band position of symmetric V-O can be varied in the range from 812 to 832 cm^{-1} depending upon synthesis method of $BiVO_4$ [32]. The longer Raman shift corresponds to the shorter V–O bond lengths and is believed to make the more distortion of vanadate tetrahedron. The greater degree of distortion of vanadate ion, the more overlap between Bi 6s and O 2p orbitals which contributes to the enhancement of photogenerated hole migration [33].

It is well-known that the optical absorption ability of materials is one of the key factors for determining photocatalytic ability. The more photons are absorbed, the more electrons and holes will be generated, and thus leading to more efficient photocatalytic reactions [17]. Hence, UV/Vis absorption of various $BiVO_4$ thin films deposited on FTO substrate was carried out. Both MIX- and H_2O-BVO samples are found to display strong absorption in the visible light region (Fig. 4a). Such absorption profile is characteristic of monoclinic $BiVO_4$. Since the absorbance value might be correlated to the quantity of materials in the film, it can be confirmed that both H_2O-BVO and MIX-BVO have similar thicknesses (See the cross-sectional view of FESEM images in Fig. 1b and c). A slightly lower absorbance of H_2O-BVO might originate from the higher roughness surface of H_2O-BVO film than that of MIX-BVO. The denser and less rough of MIX-BVO film obtained in this work may reduce the light scattering and then enhance the transmission of light, contributing to the increase of electron transition between conduction and valence band [11,34]. As a result, more electrons and holes participated in the reaction at the interface of $BiVO_4$ and electrolyte that could enhance the PEC performance. Band gap (E_g) of $BiVO_4$ can be determined by Tauc plot as present in Fig. S6. The obtained result yields a band gap value of approximately 2.4 eV, which is in good agreement with other reports [5,12]. There is only a very slight difference between values of band gap between MIX-BVO and H_2O-BVO. MIX-BVO has a slightly larger band gap value than that for $BiVO_4$ obtained by the conventional hydrothermal process, probably due to the confinement effects for its small particle size and internal lattice distortions [35].

Photoluminescence (PL) spectra were measured for further understanding the dynamics of photogenerated electron-hole pairs, including the charge transfer, recombination, and defect trapping processes [36]. In general, for the band to band PL spectra, the weaker PL intensity, the higher charge separation efficiency [37,38]. As in Fig. 4b, H_2O-BVO film shows a broad emission peak which can be ascribed to the recombination of electron in V 3d band and hole from the hybrid orbitals of Bi 6s and O 2p. Apparently, PL emission intensity of MIX-BVO sample is significantly reduced comparing with that of H_2O-BVO, which indicates the better separation of electrons and holes of MIX-BVO film. In other words, surface recombination on MIX-BVO photoelectrode can be regarded to be nearly completely suppressed. It is assumed that the compact and the less rough film might decrease the required distance for electron transport, and thus reduced the electron-hole recombination and enhanced the photocurrent density [34]. It should be mentioned that although it can not be ruled out that the excitonic PL process in which the non-radiative transitions of excited electrons from the CB bottom to different sub-bands (or surface states) might occur simultaneously, leading to PL emission from bulk $BiVO_4$ might be quenched partially, MIX-BVO is strongly believed to have superior charge separation and transfer properties which will be discussed in detail hereinafter (Fig. 7).

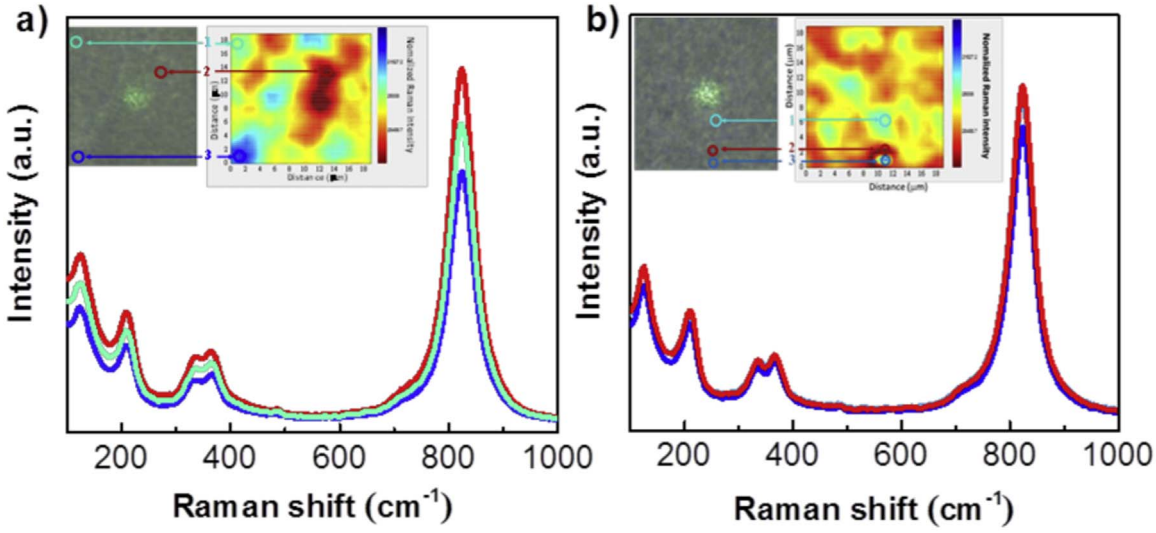

Fig. 3. Raman spectra obtained at marked spots on of H_2O-BVO (a) and MIX-BVO (b). The insets are microphotographs of the area (20 μm×20 μm) where the Raman imaging was taken.

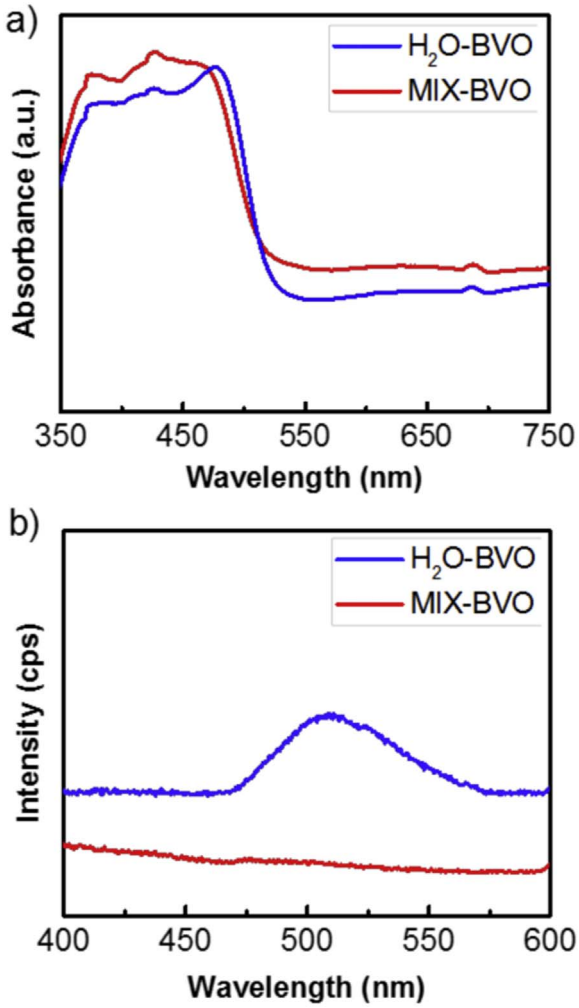

Fig. 4. Normalized UV/Vis absorption of MIX-BVO and H_2O-BVO (a) and photoluminescence (PL) spectra of $BiVO_4$ films measured with excitation at 325 nm (b).

3.2. Contribution of EG to crystalline quality and PEC performance

On the basis of the previous physicochemical characterizations, it is helpful to presume that there are various reasons behind the much better characteristics and catalytic performance of MIX-BVO than that of H_2O-BVO films. First, the slow growth kinetics of $BiVO_4$ in the mixture of EG and water is believed to attribute to homogeneity and high crystallinity of MIX-BVO samples. The formation process of $BiVO_4$ film on FTO glass in such condition is proposed in Fig. 5. Ethylene glycol has been considered as an effective reaction solvent due to its special physical and chemical properties. The high permittivity allows it to dissolve highly polar inorganic and organic compounds and the relatively strong chelating ability makes it easy to form complexes with transition metals [29,39–41]. Hence, cations in the reaction mixture may be trapped in the network of hydrogen bonds, located between two adjacent hydroxyls group in EG which assist nucleation and control the crystal growth. Therefore, in our study, EG was utilized for the hydrothermal process. We proposed that, at room temperature, Bi^{3+} ions firstly interacted with EG to form a homogeneous and transparent solution consisting of alkoxide complexes ($Bi(OCH_2CH_2OH)^{2+}$). No precipitation was observed which was different from that in the aqueous system [42]. Under the hydrothermal process, Bi^{3+} was gradually released upon dissociation of the complex. Subsequently, VO_4^{3-} ion reacted with Bi^{3+} to form $BiVO_4$ nuclei and grew into the primary $BiVO_4$ colloidal nanoparticles and then strongly attached to the seed layer. Moreover, the addition of EG helped increase the viscosity of the solution matrix, so that aggregation of $BiVO_4$ nanoparticles in the mixed solvent system was kinetically slower, leading to the slow growth of $BiVO_4$ nuclei. The growth rate reduction caused by EG might be related to changes in ionic strength, interfacial tension, and dehydration process [43]. Therefore, the nanocrystals can rotate to find the low energy configuration interface and form perfectly oriented crystals [29]. As a result, a better control over the homogeneous distribution of high crystalline could be achieved. In contrast, when water was used as the only solvent, there was no such viscosity and crystal growth inhibitory effect, resulting in a faster growth of microstructure and subsequently thicker films.

Additionally, surface wettability, well-known to have a significant influence on the PEC performance [34], was enhanced highly by the ethylene-assisted hydrothermal produced MIX-BVO photoelectrode. Indeed, MIX-BVO and H_2O-BVO photoanodes showed an apparent hydrophilicity difference (Fig. 6), with contact angles of 53.8° ± 6.4 and 111.3° ± 5.7, respectively. Better hydrophilicity of the MIX-BVO surface could facilitate the aqueous electrolyte immersing into films and lead to the better interaction between aqueous electrolyte and photoelectrode. Consequently, oxidation reaction at the semiconductor-electrolyte interface could be promoted owing to the enhancement of

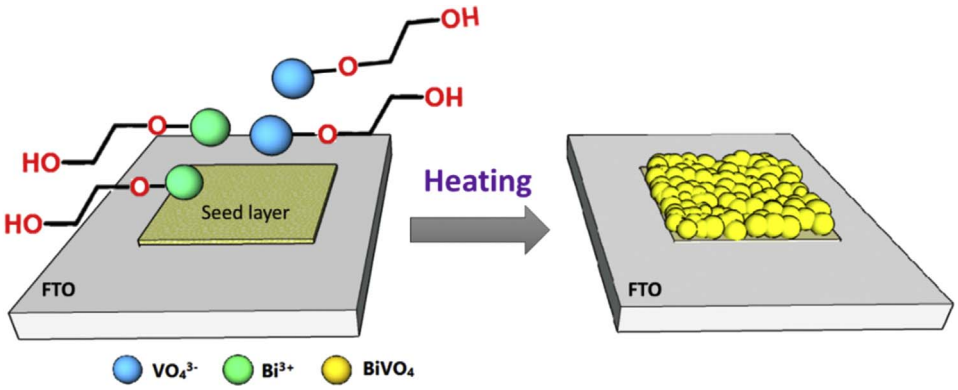

Fig. 5. Schematic diagram of the formation mechanism of the $BiVO_4$.

surface reaction kinetics and carrier separation [18].

3.3. Photoelectrochemical performance of $BiVO_4$ electrode

The photocatalytic performance of the $BiVO_4$ was evaluated by using as-prepared films as anodes for the PEC water oxidation reaction. First, to give the readers a sense of the context that the water oxidation reaction plays in state-of-the-art PEC solar fuel production, it is helpful to briefly summarize the operation mechanism of a PEC device. When a semiconductor absorbs photons with energy equal to or greater than its band gap, electrons will be excited from valence band (VB) to the conduction band (CB), leaving holes in the valence band and excess electrons in the conduction band. These electron-hole pairs play key roles in the redox reactions of water splitting. The holes left behind in the VB migrate to the surface to carry out oxidation processes to generate oxygen at the photoanode surface while hydrogen is simultaneously formed at the cathode *via* water reduction by the electrons. The cleavage of water molecules to form O_2 and H_2 can, therefore, be represented by the following redox half reactions:

$$4H^+ (aq) + 4e^- \rightarrow 2H_2 (g)\ E°=0V\ vs.\ NHE \quad (2)$$

$$2H_2O (l) + h^+ \rightarrow O_2 (g) + 4H^+ (aq) + 4e^-\ E°=1.23V\ vs.\ NHE \quad (3)$$

The water oxidation half-reaction is considered to be a bottleneck for acquiring highly efficient solar-driven water splitting due to the requisite of four protons and four electrons to yields bond-making steps and sluggish kinetics [44]. As a result, the rate at which a material can catalyze water oxidation reaction by facilitating O–O bond formation is a key determinant of the overall efficiency of water splitting. In this work, we, therefore, take more effort to understanding and overcoming the limitations of the water oxidation reaction on $BiVO_4$ electrodes for solar fuel production.

One reported that it would not be practical to run a large-scale energy conversion system at an applied bias larger than 1.6 V *vs.* RHE (pH 7) because the energy input required to sustain the bias would compromise the energy output [45]. Furthermore, the thermodynamic water oxidation potential is also less than 1.6 V *vs.* RHE. Therefore, all J-E curves (both LSV and CV scans) shown in Fig. 7 and Fig. S7, respectively, were run from −0.15 to +1.4 V *vs.* RHE (−0.6–0.7 V *vs.* Ag/AgCl at pH 9.3, correspondingly). Additionally, the photocurrent density at 1.23 V *vs.* RHE and the onset potential were taken as the criteria to compare the performances of various $BiVO_4$ electrodes. At first glance, the dark current density for both MIX- and H_2O-BVO films are close to zero, which suggests that the natural surface of $BiVO_4$ can not oxidize water efficiently without applying high enough overpotential. However, it can be clearly seen that the photo-induced current density of MIX-BVO electrode is a function of applied voltage in 0.1 M $Na_2B_4O_7$ solution under AM1.5G simulated sunlight irradiation (Fig. 7a). Photocurrent density rose quite linearly with the rising of bias potential (anodic sweep), indicating that surface recombination effect is significantly suppressed to a certain degree. At 1.23 V *vs.* RHE, photo-induced current density achieved at *ca.* 1.04 ± 0.07 mA cm^{-2}. These photocurrent density patterns clearly illustrate that $BiVO_4$ is n-type anodic electrode. The photocurrents in this work are among the highest results reported in the literature for pure $BiVO_4$ (those without heterojunction, composition tuning, impurities doping or co-catalyst) in the absence of the sacrificial agent or hole/electron scavenger (Table S1). To guarantee the superior performance of MIX-BVO is reliable and reproducible, ten different devices were fabricated and tested at the separate period of time. It is noteworthy that the PEC activity of MIX-BVO electrode is almost ten times higher that of H_2O-BVO, which is only about 0.07 mA cm^{-2}. Considering that the H_2O-BVO film shows similar thickness and has the same crystal phase, the poorer performance of the H_2O-BVO must be a consequence of its slightly lower absorption, poor crystallinity and higher recombination rate which have been affirmed from above characterization results. Besides, H_2O-BVO showed slight decrease trend in photocurrent is probably due to the recombination rate of charge carriers exceeds the rate at which the electrons can be generated. Interestingly, the onset potential at *ca.* 0.4 V *vs.* RHE in this work is also lower than other previous reports which are typically in the range of 0.5–0.6 V *vs.* RHE [46,47]. This distinct onset potential indicates the influence of surface recombination process, which is usually dominant at lower bias [48], is suppressed to a certain degree. Our PEC performance results suggest

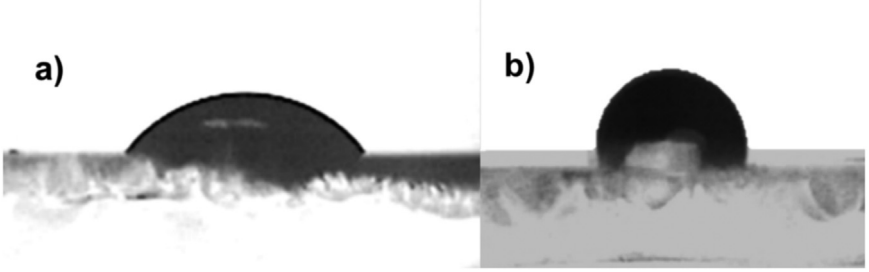

Fig. 6. Surface water contact angle of MIX-BVO (a) and H_2O-BVO (b) films.

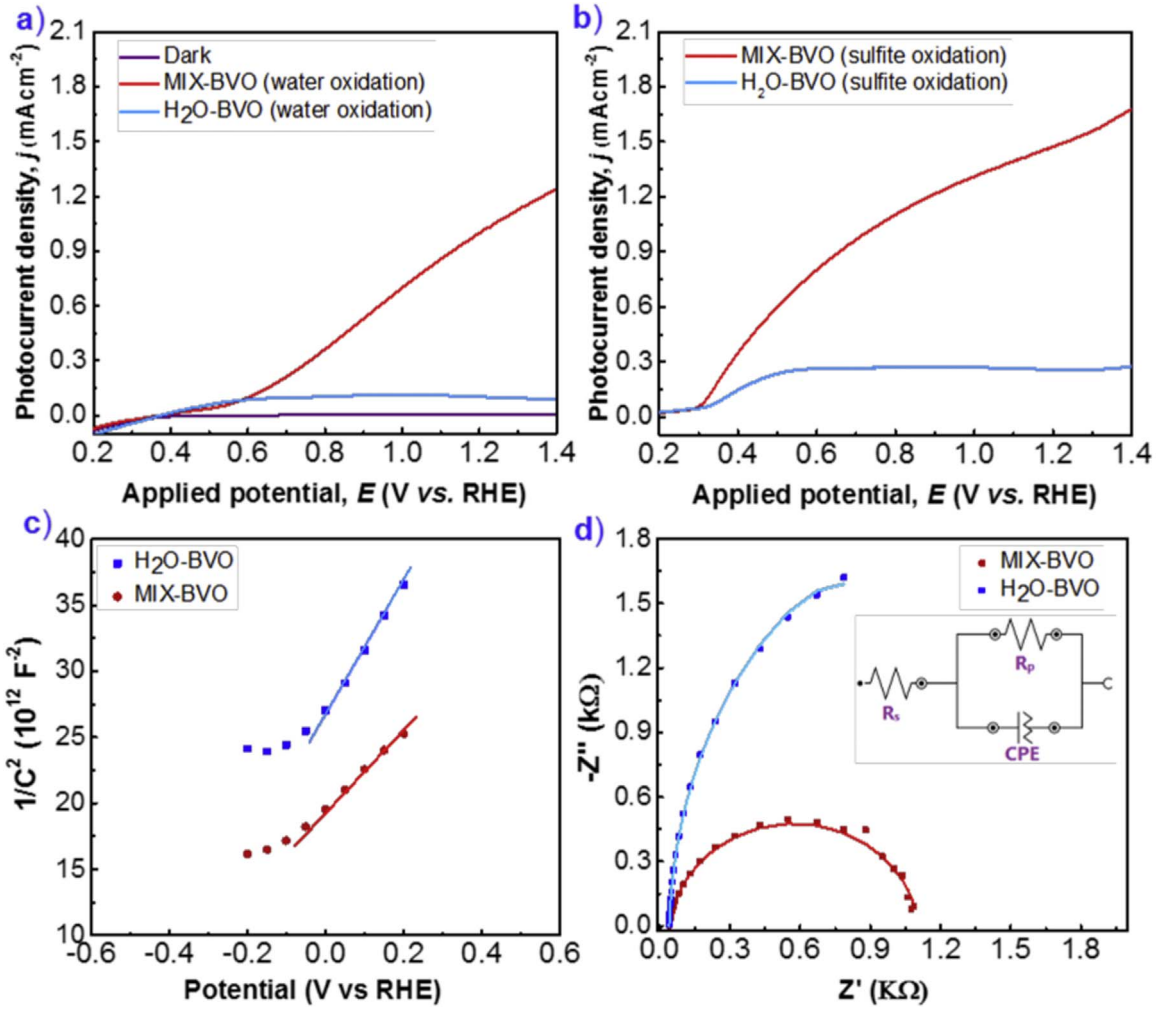

Fig. 7. J-E curves for (a) water oxidation (0.1 M $Na_2B_4O_7$) and (b) sulfite oxidation (0.1 M Na_2SO_3 +0.1 M $Na_2B_4O_7$) using the MIX-BVO and H_2O-BVO as photoanode under visible light irradiation; (c) Mott–Schottky plots for photoanodes measured at a frequency of 1 kHz and amplitude of 10 mV in 0.1 M $Na_2B_4O_7$ in the dark. (d) Nyquist plots of the photoanodes under illumination. The solid line was fitted by Nova software using the equivalent circuit model (the inset).

that besides the suitable band gap and optical absorption ability, crystallinity and surface hydrophilicity of monoclinic $BiVO_4$ also play a crucial role in determining their photocatalytic water splitting performance. The more photons are absorbed, the more electron and hole pairs are generated, and the higher efficient photocatalytic ability will be achieved [17]. Increasing in crystallinity results in the increase in the delocalization of the electron and hole pairs and greater overlapping between the Bi 6s and O 2p orbitals, which enhances the O_2 evolution activity of $BiVO_4$ [49].

For a more quantitative discussion, the oxidation efficiency (η_{ox}) of the photoanodes by photogenerated holes which is closely related to carrier recombination on the surface was studied. Since oxidation of sulfite ($SO_3^{2-}/SO_3^{\cdot-}$, E°=0.73 V *vs.* NHE; $SO_3^{2-}/S_2O_6^{2-}$, E° =0.026 V *vs.* NHE) is favored over water oxidation, both thermodynamically and kinetically, the surface recombination losses due to slow interfacial hole transfer kinetics can be assumed negligible for photo-oxidation of sulfite [24]. Therefore, the oxidation efficiency (η_{ox}) was calculated by comparing the photocurrent for sulfite oxidation and water oxidation (the details for η_{ox} calculation are given in the ESI, Fig. S9). As depicted in Fig. 7b, J-E curves show a significant improvement in both the onset potential and photocurrent density in the presence of the hole-scavenging sulfite. Accordingly, at 1.23 V *vs.* RHE, oxidation efficiency of MIX-BVO photoanode was found to be about 73.1%, nearly three times higher than the corresponding value for H_2O-BVO (25.9%) (see Fig. S9). The much higher n_{ox} of MIX-BVO indicates that most of the holes are transferred to the electrode/electrolyte interface and participated in oxidation reaction under visible irradiation. In other words, most of the holes from H_2O-BVO electrode are wasted in recombination on the surface instead of contributing to the water oxidation reaction. The better yield of charge injection of MIX-BVO could result from the better interfacial contact between electrolyte and electrode surface. Importantly, an early onset potential (0.28 V *vs.* RHE) and a rapid increase in photocurrent for sulfite oxidation on the MIX-BVO electrode indicated an excellent fill factor [24].

Mott–Schottky (M-S) analysis is thereby conducted at a frequency of 1 kHz on both MIX- and H_2O-BVO in 0.1 M $Na_2B_4O_7$ electrolyte in the dark from which donor density can be estimated using the slope of the linear region (See Fig. 7c and also SI for a detailed description). As expected for n-type semiconductor, both samples showed positive slopes. In comparison to H_2O-BVO, MIX-BVO showed a smaller slope indicating a significantly enhanced donor density. Accordingly, the carrier density of MIX-BVO and H_2O-BVO was estimated approximately to be 5.1×10^{18} cm^{-3} and 3.4×10^{18} cm^{-3}, respectively. The increased donor density is expected to shift Fermi level of MIX-BVO toward the conduction band and accelerate the charge transfer at the interface of $BiVO_4$ and FTO substrate by increasing the band bending [50]. Consequently, the PEC performance of MIX-BVO was thereby enhanced remarkably. Hence, in order to explore the origin of the enhanced PEC performances and discover the interfacial charge transfer properties, electrochemical impedance spectroscopy (EIS)

was also conducted. Here, the EIS data were measured using a three-electrode cell system, thus the arc in Nyquist plot indicates the charge transfer kinetics on the working electrode and the diameter of the semicircle reflects the charge transfer resistance. As depicted in Fig. 7d, MIX-BVO exhibits smaller impedance arc diameter than that of H_2O-BVO. The decrease of arc in an EIS Nyquist plot represents the charge transport across MIX-BVO/electrolyte interface is more favorable. The higher charge transfer ability at the interface between photoelectrode/electrolyte diminishes the charge recombination and induces the facile charge transport of electrons through the films [19]. This is in good agreement with the higher carrier density of the MIX-BVO than the H_2O-BVO, as evidenced by M-S analysis shown in Fig. 7c. In addition to the lower charge transfer resistance (R_{CT}) value, the charge transfer capacitance (CPE) value of MIX-BVO is also found to be higher than H_2O-BVO. The charge transfer capacitance is related to the surface states, and a higher capacitance value indicates a greater surface density of states. However, from the aspect of the role of surface states, till now, it remains controversial. On one hand, surface states might act as trapping site, thereby are often thought to be limit photovoltaic and photocatalytic performance. On the other hand, one may also argue that surface states are able to facilitate charge separation and help localize charges closing to the semiconductor interface, thereby enhancing the performance [51,52]. In this work, we proposed that the higher surface states of MIX-BVO imply that MIX-BVO could have a stronger dipole that might attract a greater amount of water molecules, thus resulting in an increase in photoelectrocatalytic performance and photocurrent.

While the three-electrode system described above is sufficient to compare our results to others in the literature, a two-electrode configuration should be done to accurately measure cell efficiency. Herein, incident photon-to-electron conversion efficiency (IPCE), which is known as a critical index to study light conversion efficiency [53], was also obtained to assess the contribution of monochromatic light to the current density at wavelengths ranging from 350 to 600 nm in 1 M $Na_2B_4O_7$ solution (Fig. 8). The onset of the IPCE of MIX-BVO can reach 500 nm, which is close to its light absorption edge (510 nm), implying that the anodic photocurrent attributed to the band gap transition [54]. Apparently, the MIX-BVO exhibits significantly enhanced IPCE in comparison with H_2O-BVO from UV extending to the visible region. The IPCE value of the former reaches about 20% at 420 nm, which is nearly 10 times as high as the latter. Subsequently, the absorbed photon-to-current efficiency (APCE) of MIX-BVO at 420 nm is over ten-time higher than that of H_2O-BVO, revealing that absorbed photons can be utilized more efficiently, due to the improved

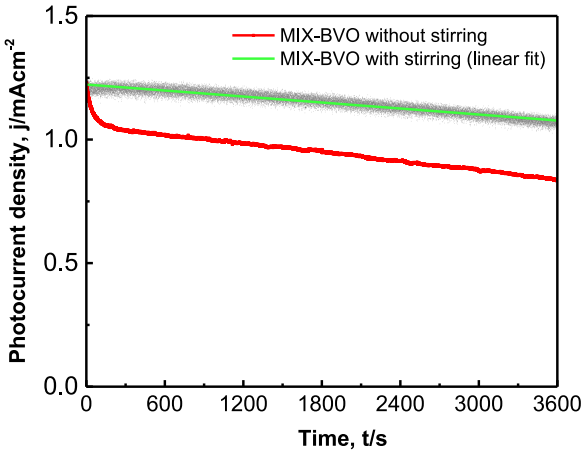

Fig. 9. Chronoamperometry of $BiVO_4$ films at 0.6 V *vs.* Ag/AgCl under AM 1.5 G 1 sun illumination.

charge separation. To the best of our knowledge, our result is among the state-of-art IPCE that is larger than 20% in the absence of sacrificial agents [23]. For instance, Alarcón-Lladó *et al.* observed IPCE about 10% for wavelengths below 450 nm while Berglund et al. reported IPCE values above 14% for 340–460 nm light for nanoporous $BiVO_4$ films. The highest efficiency was reported to be 29% at 420 nm achieved by nanocrystalline $BiVO_4$ film electrode [55].

To be practically applied in a large-scale PEC energy conversion system, it is mandatory for the material to remain stable for extended periods of time under illumination. However, there are only a few reports in the literature examining the long-term stability of $BiVO_4$ film. Herein, we conducted long-term PEC test of $BiVO_4$ films in borate solutions with a constant potential of +1.35 V *vs.* RHE (corresponding to 0.6 V *vs.* Ag/AgCl, pH 9.3) as shown in Fig. 9. There was about 30% photocurrent density decrease observed after 1 h of $BiVO_4$ in the unstirred electrolyte. During the stability testing, gaseous oxygen bubbles were obviously generated and partially accumulated on the working electrode surface, reducing the surface area available for PEC reaction [45]. Furthermore, the bubbles growing on the electrode surface lowered the conductivity and increased the resistance of the electrolysis cell. Both these factors would affect the working potential of the photoelectrochemical cell [56]. Therefore, in order to prevent bubbles accumulation on the electrode surface, the electrolyte solution was stirred gently. Interestingly, the decay of photocurrent density decreased to only 11% which is well consistent with our above

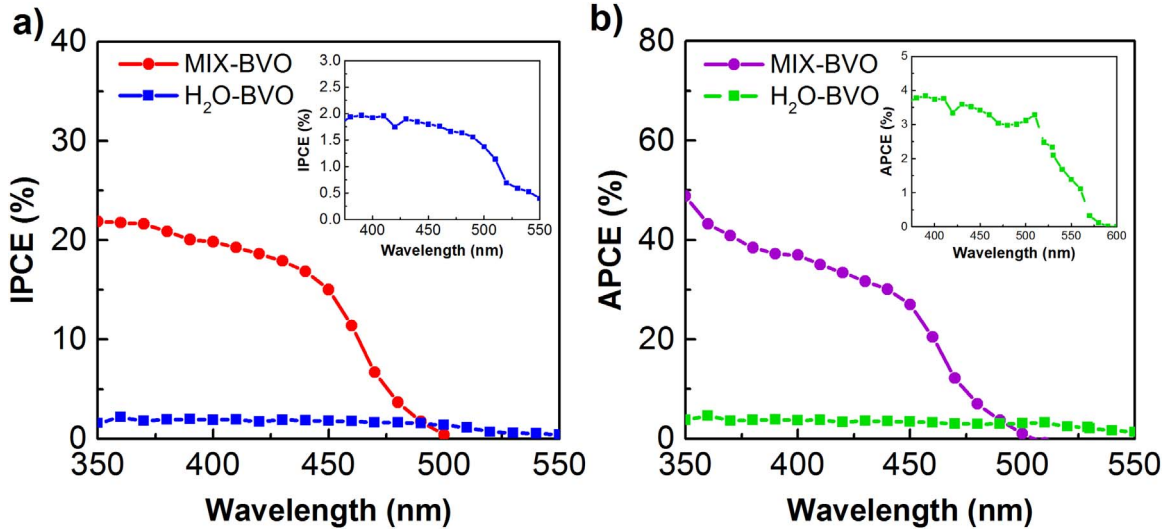

Fig. 8. IPCE (a) and APCE (b) of MIX-BVO (•) and H_2O-BVO (■) measured in 0.1 M $Na_2B_4O_7$ at 1 V *vs.* Pt under AM 1.5G 1 sun illumination.

assumption and it is one of the best among reports [41,54].

In addition, the change in chemical composition on the electrode surface might cause a fraction of photocurrent density decay. Hence, XPS was performed to measure the composition of the film surface before and after stability testing. Two main symmetric peaks, Bi $4f_{7/2}$ and Bi $4f_{5/2}$, are found at 159.0 eV and 164.2 eV, assigned to Bi^{3+}(Fig. S12) while V $2p_{3/2}$ and V $2p_{1/2}$ can be observed at binding energy of 516.8 and 524.2 eV, which can be assigned to V^{5+}. In our samples, no evidence for the existence of V^{4+}, which is expected to have a binding energy of 515.5–516.0 eV. O 1 s spectra evidenced a peak at 530.2 eV and broad small peak at around 532–535 eV. These peaks represent the lattice oxygen (Bi-O) and absorbed oxygen on the surface. After long-term stability testing, the intensity of these peaks had changed. Such behavior is consistent with prior observations of the catalyst dissolution. For instance, Ding et al. reported that the V/Bi ratio was decreased to 0.1 after 4 h reaction [57]. Nevertheless, it is worth stating that XPS might not measure the concentration and oxidation states of elements below the surface. Hence, EDS characterization technique which can measure elements composition in bulk material was employed. As shown in (Fig. S13), MIX-BVO film has been formed and deposited in the correct stoichiometry and almost did not change during the stability test, suggesting that only the material at the top surface was dissolved.

4. Conclusions

In this study, the monoclinic $BiVO_4$ thin films with high crystalline, well distribution and strong adhesion were successfully fabricated on FTO substrate through a hydrothermal process with the mediation of EG. SEM and XRD indicated that the optimized $BiVO_4$ film had a monoclinic crystal structure and it was composed of compact sub-micron-particles. Under simulated AM 1.5G illumination, the MIX-BVO electrode attained more than 15-fold higher in photocurrent density at an applied potential of 1.23 V *vs*. RHE that of H_2O-BVO film. Additionally, the EG-assisted growth mechanism of the $BiVO_4$ film and its contribution to PEC performance, including higher wettability, homogeneity in local structure and better charge transfer, have also been discussed. Based on the above analyses, the as-synthesized MIX-BVO film is not only well appropriate for using as photoelectrode in water oxidation, but might also in other applications including photo-electrocatalytic decomposition of organic pollutants, biosensors or dye-sensitized solar cells. Furthermore, this synthesis approach is applicable to synthesize other binary oxide films.

Acknowledgement

This research was supported by Ministry of Science and Technology, R.O.C. (MOST 105-2221-E-011-143). We also acknowledge the support from National Taiwan University of Science and Technology.

Appendix A. Supplementary material

Supplementary data associated with this article can be found in the online version at http://dx.doi.org/10.1016/j.solmat.2017.03.012.

References

[1] J.-Q. Li, Z.-Y. Guo, D.-F. Wang, H. Lui, J. Du, Z.-F. Zhu, Effects of pH value on the surface morphology of $BiVO_4$ microspheres and removal of methylene blue under visible light, J. Exp. Nanosci. 9 (2012) 616–624.
[2] G. Li, D. Zhang, J.C. Yu, Ordered mesoporous $BiVO_4$ through nanocasting: a superior visible light-driven photocatalyst, Chem. Mater. 20 (2008) 3983–3992.
[3] B. Liu, Y. Fang, Z. Li, S. Xu, Visible-light nanostructured photocatalysts – a review, J. Nanosci. Nanotechnol. 15 (2015) 889–920.
[4] M. Pelaez, N.T. Nolan, S.C. Pillai, M.K. Seery, P. Falaras, A.G. Kontos, P.S.M. Dunlop, J.W.J. Hamilton, J.A. Byrne, K. O'Shea, M.H. Entezari, D.D. Dionysiou, A review on the visible light active titanium dioxide photocatalysts for environmental applications, Appl. Catal. B Environ. 125 (2012) 331–349.
[5] A. Loiudice, J. Ma, W.S. Drisdell, T.M. Mattox, J.K. Cooper, T. Thao, C. Giannini, J. Yano, L.W. Wang, I.D. Sharp, R. Buonsanti, Bandgap tunability in Sb-alloyed $BiVO_4$ quaternary oxide ass visible light absorbers for solar fuel applications, Adv. Mater. 27 (2015) 6733–6740.
[6] X. Chen, W. Shangguan, Hydrogen production from water splitting on CdS-based photocatalysts using solar light, Front. Energy 7 (2013) 111–118.
[7] M. Barawi, I.J. Ferrer, J.R. Ares, C. Sánchez, Hydrogen evolution using palladium sulfide (PdS) nanocorals as photoanodes in aqueous solution, ACS Appl. Mater. Interfaces 6 (2014) 20544–20549.
[8] J. Liang, Y. Yang, J. Zhang, J. Wu, P. Dong, J. Yuan, G. Zhang, J. Lou, Metal diselenide nanoparticles as highly active and stable electrocatalysts for the hydrogen evolution reaction, Nanoscale 7 (2015) 14813–14816.
[9] Z. Pan, I. Mora-Seró, Q. Shen, H. Zhang, Y. Li, K. Zhao, J. Wang, X. Zhong, J. Bisquert, High-efficiency "green" quantum dot solar cells, J. Am. Chem. Soc. 136 (2014) 9203–9210.
[10] W. Li, Z. Pan, X. Zhong, $CuInSe_2$ and $CuInSe_2$–ZnS based high efficiency "green" quantum dot sensitized solar cells, J. Mater. Chem. A 3 (2015) 1649–1655.
[11] S. Xiao, H. Chen, Z. Yang, X. Long, Z. Wang, Z. Zhu, Y. Qu, S. Yang, Origin of the different photoelectrochemical performance of mesoporous $BiVO_4$ photoanodes between the $BiVO_4$ and the FTO side illumination, J. Phys. Chem. C 119 (2015) 23350–23357.
[12] J.H. Kim, J.S. Lee, $BiVO_4$-based heterostructured photocatalysts for solar water splitting: a review, Energy Environ. Focus. 3 (2014) 339–353.
[13] C. Xu, G. Zhu, J. Wu, J. Liang, Template-free hydrothermal synthesis different morphologies of visible-light-driven $BiVO_4$ photocatalysts, J. Nanosci. Nanotechnol. 14 (2014) 4475–4480.
[14] J. Resasco, H. Zhang, N. Kornienko, N. Becknell, H. Lee, J. Guo, A.L. Briseno, P. Yang, TiO_2/$BiVO_4$ nanowire heterostructure photoanodes based on type II band alignment, ACS Cent. Sci. 2 (2016) 80–88.
[15] A. Galembeck, O.L. Alves, $BiVO_4$ thin film preparation by metalorganic decomposition, Thin Solid Films 365 (2000) 90–93.
[16] D.K. Zhong, S. Choi, D.R. Gamelin, Near-complete suppression of surface recombination in solar photoelectrolysis by "co-Pi" catalyst-modified W: $bivo_4$, J. Am. Chem. Soc. 133 (2011) 18370–18377.
[17] T. Huo, X. Zhang, X. Dong, X. Zhang, C. Ma, G. Wang, Photonic crystal coupled porous $BiVO_4$ hybrid for efficient photocatalysis under visible light, J. Mater. Chem. A 2 (2014) 17366–17370.
[18] C. Feng, Z. Jiao, S. Li, Y. Zhang, Y. Bi, Facile fabrication of $BiVO_4$ nanofilms with controlled pore size and their photoelectrochemical performances, Nanoscale 7 (2015) 20374–20379.
[19] S.J. Hong, S. Lee, J.S. Jang, J.S. Lee, Heterojunction $BiVO_4$/WO_3 electrodes for enhanced photoactivity of water oxidation, Energy Environ. Sci. 4 (2011) 1781.
[20] E. Alarcón-Lladó, L. Chen, M. Hettick, N. Mashouf, Y. Lin, A. Javey, J.W. Ager, $BiVO_4$ thin film photoanodes grown by chemical vapor deposition, Phys. Chem. Chem. Phys. 16 (2014) 1651–1657.
[21] W. Luo, Z. Wang, L. Wan, Z. Li, T. Yu, Z. Zou, Synthesis, growth mechanism and photoelectrochemical properties of $BiVO_4$ microcrystal electrodes, J. Phys. D. Appl. Phys. 43 (2010) 405402.
[22] M.R. da Silva, L.V.A. Scalvi, V.S.L. Neto, L.H. Dall'Antonia, Dip-coating deposition of resistive $BiVO_4$ thin film and evaluation of their photoelectrochemical parameters under distinct sources illumination, J. Solid State Electrochem. 20 (2016) 1–12.
[23] Y. Liang, T. Tsubota, L.P.A. Mooij, R. Van De Krol, Highly improved quantum efficiencies for thin film $BiVO_4$ photoanodes, J. Phys. Chem. C 115 (2011) 17594–17598.
[24] K.J. McDonald, K.-S. Choi, A new electrochemical synthesis route for a BiOI electrode and its conversion to a highly efficient porous $BiVO_4$ photoanode for solar water oxidation, Energy Environ. Sci. 5 (2012) 8553.
[25] D. Kang, Y. Park, J.C. Hill, K.S. Choi, Preparation of Bi-based ternary oxide photoanodes $BiVO_4$, Bi_2WO_6, and $Bi_2Mo_3O_{12}$ using dendritic Bi metal electrodes, J. Phys. Chem. Lett. 5 (2014) 2994–2999.
[26] P. Brack, J.S. Sagu, T.A.N. Peiris, A. McInnes, M. Senili, K.G.U. Wijayantha, F. Marken, E. Selli, Aerosol-assisted CVD of bismuth vanadate thin films and their photoelectrochemical properties, Chem. Vap. Depos. 21 (2015) 41–45.
[27] O. Schäf, H. Ghobarkar, P. Knauth, Hydrothermal synthesis of nanomaterials, in: P. Knauth, J. Schoonman (Eds.), Nanostructured Mater, Springer, US, 2002, pp. 23–41.
[28] H. Gong, N. Freudenberg, M. Nie, R. Van De Krol, K. Ellmer, $BiVO_4$ photoanodes for water splitting with high injection efficiency, deposited by reactive magnetron co-sputtering, AIP Adv. 6 (2016) 45108.
[29] L. Chen, J. Wang, D. Meng, Y. Xing, C. Wang, F. Li, Y. Wang, X. Wu, Enhanced photocatalytic activity of hierarchically structured $BiVO_4$ oriented along {040} facets with different morphologies, Mater. Lett. 147 (2015) 1–3.
[30] J. Yu, Y. Zhang, A. Kudo, Synthesis and photocatalytic performances of $BiVO_4$ by ammonia co-precipitation process, J. Solid State Chem. 182 (2009) 223–228.
[31] J. Liu, H. Wang, S. Wang, H. Yan, Hydrothermal preparation of $BiVO_4$ powders, Mater. Sci. Eng. B Solid-State Mater. Adv. Technol. 104 (2003) 36–39.
[32] H.K. Timmaji, W. Chanmanee, N.R. De Tacconi, K. Rajeshwar, Solution combustion synthesis of $BiVO_4$ nanoparticles: effect of combustion precursors on the photocatalytic activity, J. Adv. Oxid. Technol. 14 (2011) 93–105.
[33] J. Yu, A. Kudo, Effects of structural variation on the photocatalytic performance of hydrothermally synthesized $BiVO_4$, Adv. Funct. Mater. 16 (2006) 2163–2169.
[34] X. Liu, Y. Liu, J. Su, M. Li, L. Guo, Facile preparation of $BiVO_4$ nanoparticle film by electrostatic spray pyrolysis for photoelectrochemical water splitting, Int. J. Hydrog. Energy 40 (2015) 12964–12972.

[35] Q. Luo, L. Zhang, X. Chen, O.K. Tan, K.C. Leong, Mechanochemically synthesized m-$BiVO_4$ nanoparticles for visible light photocatalysis, RSC Adv. 6 (2016) 15796–15802.
[36] H.L. Tan, X. Wen, R. Amal, Y.H. Ng, $BiVO_4$ {010} and {110} relative exposure extent: governing factor of surface charge population and photocatalytic activity, J. Phys. Chem. Lett. 7 (2016) 1400–1405.
[37] D.K. Ma, M.L. Guan, S.S. Liu, Y.Q. Zhang, C.W. Zhang, Y.X. He, S.M. Huang, Controlled synthesis of olive-shaped Bi_2S_3/$BiVO_4$ microspheres through a limited chemical conversion route and enhanced visible-light-responding photocatalytic activity, Dalton Trans. 41 (2012) 5581–5586.
[38] S. Dong, J. Feng, Y. Li, L. Hu, M. Liu, Y. Wang, Y. Pi, J. Sun, J. Sun, Shape-controlled synthesis of $BiVO_4$ hierarchical structures with unique natural-sunlight-driven photocatalytic activity, Appl. Catal. B Environ. 152–153 (2014) 413–424.
[39] H. Li, K. Yu, X. Lei, B. Guo, H. Fu, Z. Zhu, Hydrothermal synthesis of novel MoS_2/$BiVO_4$ hetero-nanoflowers with enhanced photocatalytic activity and a mechanism investigation, J. Phys. Chem. C 119 (2015) 22681–22689.
[40] M. Ge, L. Liu, W. Chen, Z. Zhou, Sunlight-driven degradation of Rhodamine B by peanut-shaped porous $BiVO_4$ nanostructures in the H_2O_2-containing system, CrystEngComm 14 (2012) 1038.
[41] L. Ma, W.H. Li, J.H. Luo, Solvothermal synthesis and characterization of well-dispersed monoclinic olive-like $BiVO_4$ aggregates, Mater. Lett. 102–103 (2013) 65–67.
[42] H. Huang, Y. He, X. Du, P.K. Chu, Y. Zhang, A general and facile approach to heterostructured core/shell $BiVO_4$/BiOI p-n junction: room-temperature in situ assembly and highly boosted visible-light photocatalysis, ACS Sustain. Chem. Eng. 3 (2015) 3262–3273.
[43] H. Ghafarian-Zahmatkesh, M. Javanbakht, M. Ghaemi, Ethylene glycol-assisted hydrothermal synthesis and characterization of bow-tie-like lithium iron phosphate nanocrystals for lithium-ion batteries, J. Power Sources 284 (2015) 339–348.
[44] Y. Tang, R. Wang, Y. Yang, D. Yan, X. Xiang, Highly enhanced photoelectrochemical water oxidation efficiency based on triadic quantum dot/layered double hydroxide/BiVO4 photoanodes, ACS Appl. Mater. Interfaces 8 (2016) 19446–19455. http://dx.doi.org/10.1021/acsami.6b04937.
[45] S.P. Berglund, D.W. Flaherty, N.T. Hahn, A.J. Bard, C.B. Mullins, Photoelectrochemical oxidation of water using nanostructured $BiVO_4$ films, J. Phys. Chem. C 115 (2011) 3794–3802.
[46] Y. Ma, S.R. Pendlebury, A. Reynal, F. le Formal, J.R. Durrant, Dynamics of photogenerated holes in undoped $BiVO_4$ photoanodes for solar water oxidation, Chem. Sci. 5 (2014) 2964.
[47] L. Chen, E. Alarcón-Lladó, M. Hettick, I.D. Sharp, Y. Lin, A. Javey, J.W. Ager, Reactive sputtering of bismuth vanadate photoanodes for solar water splitting, J. Phys. Chem. C 117 (2013) 21635–21642.
[48] M. Zhou, J. Bao, W. Bi, Y. Zeng, R. Zhu, M. Tao, Y. Xie, Efficient water splitting via a heteroepitaxial $BiVO_4$ photoelectrode decorated with Co-Pi catalysts, ChemSusChem 5 (2012) 1420–1425.
[49] S.M. Thalluri, C. Martinez Suarez, M. Hussain, S. Hernandez, A. Virga, G. Saracco, N. Russo, Evaluation of the parameters affecting the visible-light-induced photocatalytic activity of monoclinic $BiVO_4$ for water oxidation, Ind. Eng. Chem. Res. 52 (2013) 17414–17418.
[50] D.-D. Qin, T. Wang, Y.-M. Song, C.-L. Tao, Reduced monoclinic $BiVO_4$ for improved photoelectrochemical oxidation of water under visible light, Dalton Trans. 43 (2014) 7691. http://dx.doi.org/10.1039/c3dt53575d.
[51] M. Sachs, E. Pastor, A. Kafizas, J.R. Durrant, Evaluation of surface state mediated charge recombination in anatase and rutile TiO_2, J. Phys. Chem. Lett. 7 (2016) 3742–3746. http://dx.doi.org/10.1021/acs.jpclett.6b01501.
[52] B. Klahr, S. Gimenez, F. Fabregat-Santiago, T. Hamann, J. Bisquert, Water oxidation at hematite photoelectrodes: the role of surface states, J. Am. Chem. Soc. 134 (2012) 4294–4302. http://dx.doi.org/10.1021/ja210755h.
[53] W. He, R. Wang, L. Zhang, J. Zhu, X. Xiang, F. Li, Enhanced photoelectrochemical water oxidation on a $BiVO_4$ photoanode modified with multi-functional layered double hydroxide nanowalls, J. Mater. Chem. A 0 (2015) 1–6.
[54] Q. Jia, K. Iwashina, A. Kudo, Facile fabrication of an efficient $BiVO_4$ thin film electrode for water splitting under visible light irradiation, Proc. Natl. Acad. Sci. USA 109 (2012) 11564–11569.
[55] K. Sayama, A. Nomura, Z. Zou, R. Abe, Y. Abe, H. Arakawa, Photoelectrochemical decomposition of water on nanocrystalline $BiVO_4$ film electrodes under visible light, Chem. Commun. 23 (2003) 2908–2909.
[56] S.K. Mazloomi, N. Sulaiman, Influencing factors of water electrolysis electrical efficiency, Renew. Sustain. Energy Rev. 16 (2012) 4257–4263.
[57] C. Ding, J. Shi, D. Wang, Z. Wang, N. Wang, G. Liu, F. Xiong, C. Li, Visible light driven overall water splitting using cocatalyst/$BiVO_4$ photoanode with minimized bias, Phys. Chem. Chem. Phys. 15 (2013) 4589–4595.